Galaxy clusters in X-rays: the buildup of massive structures in the last 10 Gyrs, and CHEX-MATE

S. Ettori[1], H. Bourdin[2], S. De Grandi[3], F. Gastaldello[3], S. Ghizzardi[3], P. Mazzotta[2], M. Meneghetti[1], S. Molendi[3], M. Rossetti[3], M. Sereno[1], P. Tozzi[4], and the Italian component of CHEX-MATE

[1] INAF, Osservatorio di Astrofisica e Scienza dello Spazio, via Piero Gobetti 93/3, 40129 Bologna, Italy, e-mail: `stefano.ettori@inaf.it`
[2] Università degli studi di Roma "Tor Vergata", Via della Ricerca Scientifica, 1, 00133 Roma, Italy
[3] INAF, IASF, Via A. Corti 12, 20133 Milano, Italy
[4] INAF, Osservatorio Astrofisico di Arcetri, Largo E. Fermi, I-50122 Firenze, Italy

Abstract. The Italian community working on galaxy clusters proposed a coherent project to fully exploit both the proprietary and archival X-ray data of objects resolved spatially up to redshift 1.5. The project involved collaborative activities to address, in a synergetic exploitation of proprietary, archival and simulated data, the following goals: (i) the reconstruction of the gas density, temperature and metal abundance profiles in well-selected samples of clusters; (ii) to constrain with unprecedented accuracy the total and gas mass 3D distribution; (iii) the study of the accretion phenomena in the outskirts; (iv) detailed analyses of the ICM properties in the cores and their physical link with the nuclear activity in the central galaxies, also as function of the cosmic epoch; (v) the comparison between these observational constraints and the predictions from dedicated analytic models and hydrodynamical simulations. In this context, we started a new, unique project based on the collection, reduction, analysis and full scientific exploitation of the X-ray data of one of the only 2 AO-17 *XMM-Newton* "Multi-Year Heritage" programmes granted, CHEX-MATE.

Key words. Galaxies: clusters: intracluster medium - X-rays: galaxies: clusters - galaxies: clusters: general - cosmology: dark matter

1. Introduction

Clusters of galaxies provide valuable information on cosmology, from the physics driving galaxy and structure formation, to the nature of dark matter and dark energy. Their matter content reflects that of the Universe (85% dark matter, ~12% X-ray emitting gas and 3% galaxies Voit , 2005; Kravtsov & Borgani ,

2012). They are the nodes of the Cosmic Web, constantly growing through accretion of matter along filaments and via occasional mergers. Clusters are thus excellent laboratories for probing the physics of the gravitational collapse of dark matter and baryons, and for studying the non-gravitational physics that affects their baryonic component. Pristine gas

falls into the dark matter potential and is progressively heated up to temperatures of $10^7 - 10^8$ K, such that the majority of the baryons end up in the form of a fully ionized plasma, the intra-cluster medium (ICM), which produces X-ray emission through bremsstrahlung radiation and line emission. In addition, photons of the cosmic microwave background (CMB) crossing galaxy clusters are subject to inverse Compton scattering off the hot ICM electrons. This produces a spectral shift in the CMB signal, the Sunyaev-Zel'dovich (SZ) effect (Sunyaev & Zel'dovich , 1972), which is detectable at microwave wavelengths. X-ray emission and the SZ effect thus provide highly complementary diagnostics of the state of the ICM.

2. Results on thermodynamic profiles, metallicity, H_0, halo shapes, scaling relations

X-COP (Eckert et al. , 2017) is a very large program on *XMM-Newton* whose aim is to advance our understanding of the virialization region of galaxy clusters. The strategy adopted for the project is to target the most significant SZ sources in the *Planck* survey in order to combine X-ray and SZ information out to the virial radius (see Fig. 1). So far, we have published 14 refereed papers, more than half in the period covered from the ASI support. In Ghirardini et al. (2019), we present the radial profiles of the thermodynamic properties of the ICM out to the virial radius for a sample of 12 galaxy clusters selected from the *Planck* all-sky survey. We determine the universal profiles of gas density, temperature, pressure, and entropy over more than two decades in radius, in the radial range $0.01 - 2R_{500}$ (see Fig. 2). We provide average functional forms for the radial dependence of the main quantities and quantify the slope and intrinsic scatter of the population as a function of radius. We find that gas density and pressure profiles steepen steadily with radius, in excellent agreement with previous observational results. Entropy profiles beyond R_{500} closely follow the predictions for the gravitational collapse of structures. The scatter in all thermodynamical quantities reaches

a minimum in the range $[0.2 - 0.8]R_{500}$ and increases outward. Somewhat surprisingly, we find that pressure is substantially more scattered than temperature and density. These results indicate that once accreting substructures are properly excised, the properties of the ICM beyond the cooling region ($r > 0.3R_{500}$) follow remarkably well the predictions of simple gravitational collapse and require few non-gravitational corrections.

In Ettori et al. (2019), we use profiles of the gas temperature, density, and pressure that have been spatially resolved out to median values of $0.9R_{500}$, $1.8R_{500}$, and $2.3R_{500}$, respectively, to recover the hydrostatic gravitating mass profile with several methods and using different mass models (see e.g. Fig. 2). The hydrostatic masses are recovered with a relative (statistical) median error of 3% at R_{500} and 6% at R_{200}. By using several different methods to solve the equation of the hydrostatic equilibrium, we evaluate some of the systematic uncertainties to be of the order of 5% at both R_{500} and R_{200}. A Navarro-Frenk-White profile provides the best-fit in 9 cases out of 13; the remaining 4 cases do not show a statistically significant tension with it. The distribution of the mass concentration follows the correlations with the total mass predicted from numerical simulations with a scatter of 0.18 dex, with an intrinsic scatter on the hydrostatic masses of 0.15 dex.

Eckert et al. (2019) compare the hydrostatic gas fractions measured in the X-COP clusters with the expected universal gas fraction to constrain the level of non-thermal pressure support. We find that hydrostatic masses require little correction and infer a median non-thermal pressure fraction of $\sim 6\%$ and $\sim 10\%$ at R_{500} and R_{200}, respectively. Our values are lower than the expectations of hydrodynamical simulations, possibly implying a faster thermalization of the gas. If instead we use the mass calibration adopted by the *Planck* team, we find that the gas fraction of massive local systems implies a mass bias $1 - b = 0.85 \pm 0.05$ for Sunyaev-Zel'dovich-derived masses, with some evidence for a mass-dependent bias. Ettori & Eckert (2022) introduce a new model for the non-thermal pressure radial profile, and
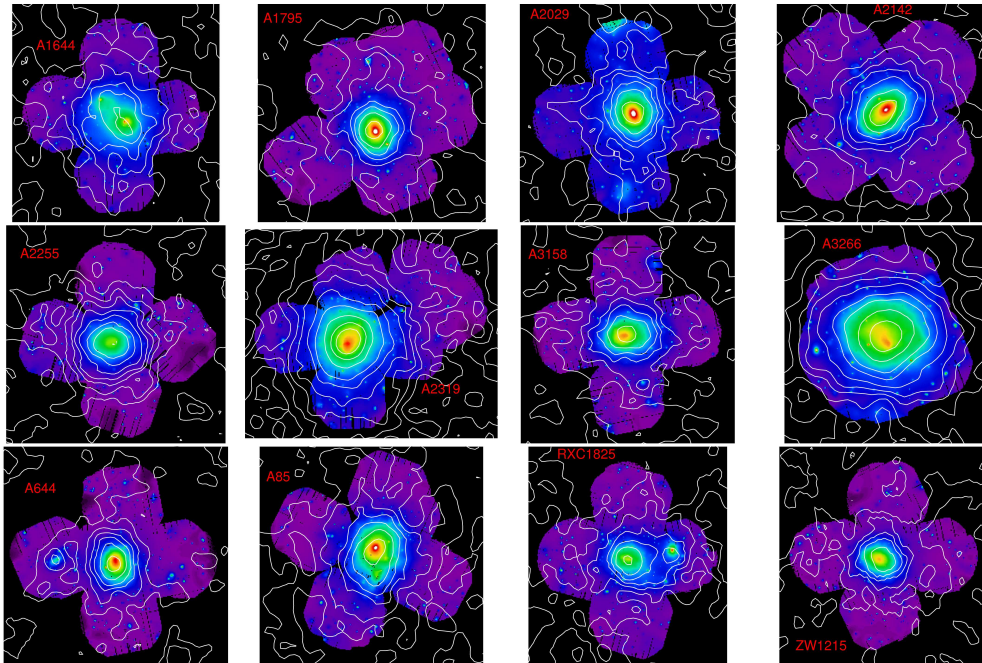
Fig. 1. Adapted from Ghirardini et al. (2019). Adaptively smoothed and exposure corrected *XMM-Newton* mosaic images in the [0.7-1.2] keV energy band for all X-COP clusters. The superimposed white contours represent the *Planck* SZ S/N maps

use data from X-COP and literature to constrain the parameters of this model, and to conclude that the recovered values of *b* are below the amount of bias required to reconcile the observed cluster number count in the cosmological framework set from *Planck*.

In Clavico et al. (2019), we analyzed a mosaic of *XMM-Newton* observations (240 ks) of the Lyra system at redshift 0.067 that is formed by the galaxy clusters pair RXC J1825.3+3026 and CIZA J1824.1+3029 (see Fig. 3), and is part of the X-COP sample. While RXCJ1825 is dynamically disturbed, with evidence of an undergoing main merger (with a mass ratio of about 1/2) in the east-west direction with an infalling galaxy group in an advanced state of disruption, CIZAJ1824 appears as a very regular undisturbed cluster. No diffuse X-ray emission is found in the region between them, indicating that these clusters are in a pre-merger phase. Southwest of RXCJ1825 there is a bright elliptical galaxy, the Southern Galaxy (SG), located at the very end of an elongated

diffuse X-ray emission joining the main cluster and this galaxy, suggesting a physical connection between the two systems. The SG hosts an X-ray-emitting gaseous corona, supporting the idea that it once was the central galaxy of a group now almost completely destroyed by interaction with RXCJ1825. Girardi et al. (2020) present the first analysis based on the kinematics of 198 member galaxies of the Lyra complex, based on new spectroscopic data for 285 galaxies acquired at the Italian Telescopio Nazionale Galileo and used in combination with PanSTARRS photometry. We confirm that the past assembly of RXCJ1825 is traced by the two dominant galaxies, which are both aligned with the major axis of the galaxy distribution along the east-west direction, and by a minor northeast substructure. We also detect a quite peculiar high velocity field in the southwest region of the Lyra complex. A dynamical analysis of the system shows that the two clusters are likely to be gravitationally bound in a pre-merger phase, and that CIZAJ1824 is mov-
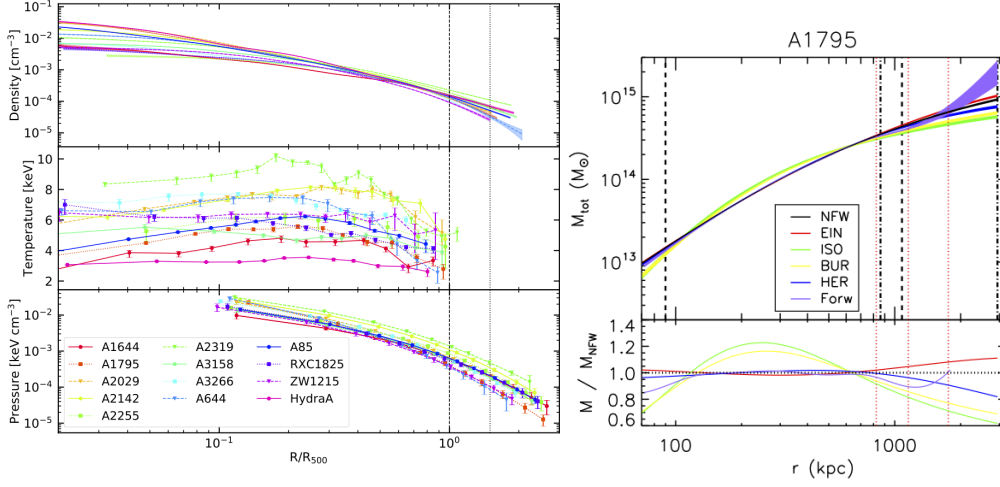
Fig. 2. (Left; from top to bottom panels) Reconstructed electron density, projected temperature, and SZ pressure profiles as functions of the radius in scale units of R_{500}. Statistical error bars are overplotted. The two vertical lines indicate R_{500} and R_{200}. (Right) Hydrostatic mass radial profiles obtained from the forward method and the mass models applied to the backward method and described in Ettori et al. (2019) (see Sect. 3.1) for A1795. Vertical lines indicate: (dotted) R_{1000}, R_{500}, and R_{200}; (dashed) third radial bin (a minimum number of three independent bins are needed to constrain a mass model with two free parameters) and upper limit in measurements of the spectroscopic temperature; (dot-dashed) radial range covered from SZ pressure profile after the exclusion of the three inner points and used in the reconstruction of the mass profile. Bottom panels: ratios of the different mass profiles to the NFW profile adopted as reference model. Adapted from Ettori et al. (2019).

ing toward RXCJ1825. The same complex has been observed with the LOw Frequency ARray (LOFAR), and a joint-analysis with the XMM exposure presented in Botteon et al. (2019). In this study, we report the discovery of a Mpc-scale radio halo with a low surface brightness extension in RXCJ1825 that follows the X-ray emission from the cluster center to the remnant of a galaxy group in the SW. This is among the least massive systems and the faintest giant radio halo known to date, and supports the merger hypothesis for RXCJ1825. In contrast to this, no diffuse radio emission is observed in CIZAJ1824 , nor in the region between the pre-merger cluster pair. The power spectra of the X-ray surface brightness fluctuations of RXCJ1825 and CIZAJ1824 are in agreement with the findings for clusters exhibiting a radio halo and clusters where no radio emission has been detected, respectively.

On the X-ray–radio correlation and the search for inverse Compton emission, Cova et

al. (2019) present the results of a joint *XMM-Newton* and NuSTAR observation (200 ks) of the galaxy cluster Abell 523 at $z = 0.104$. The peculiar morphology of the cluster radio halo and its outlier position in the radio power $P(1.4$ GHz$)$ – X-ray luminosity plane make it an ideal candidate for such a study. The thermodynamic maps obtained from the XMM observation suggest the presence of a secondary merging process that could be responsible for the peculiar radio halo morphology. This hypothesis is supported by the comparison between the X-ray and radio surface brightnesses, which shows a broad intrinsic scatter and a series of outliers from the best-fit relation, corresponding to those regions that could be influenced by a secondary merger. The global NuSTAR spectrum can be explained by purely thermal gas emission, and there is no convincing evidence that an IC component is needed.

Baldi et al. (2019) produce maps of the Comptonization parameter by applying, for the

first time, a locally parametric algorithm for sparse component separation to the latest frequency maps released by *Planck*. The algorithm takes into account properties of real cluster data through the two-component modelling of the spectral energy density of thermal dust, and the masking of bright point sources. Its robustness has been improved in the low signal-to-noise regime, thanks to the implementation of a deconvolution of *Planck* beams in the chi-square minimisation of each wavelet coefficient. The procedure is then applied to the X-COP objects, showing the presence of anisotropic features, such as small-scale blobs and filamentary substructures that are located in the outskirts of a number of clusters in the sample. The significance of their detection is established via a bootstrap-based procedure we propose here for the first time.

The combination of *XMM-Newton* and *Planck* datasets for 61 objects with redshifts up to $z < 0.5$ has allowed Kozmanyan et al. (2019) to develop a Bayesian approach that combines informed priors on the physics of the ICM obtained from hydrodynamical simulations of massive clusters with measurement uncertainties to contrain the Hubble constant H_0 with 4.4% relative error at 1σ. By applying a similar method to the X-COP objects, Ettori et al. (2020a) highlight the role of the helium abundance in assessing robustly the value of H_0.

Ghizzardi et al. (2021) present the first metal abundance profiles in the X-COP sample (see Fig. 3). Our measures extend to R_{500} and are corrected for a systematic error plaguing previous outskirt estimates. Our profiles flatten out at large radii, admittedly not a new result, however the radial range and representative nature of our sample extends its import well beyond previous findings. We find no evidence of segregation between cool-core and non-cool-core systems beyond $\sim 0.3R_{500}$, implying that, as was found for thermodynamic properties (Ghirardini et al. , 2019), the physical state of the core does not affect global cluster properties. Our mean abundance within R_{500} shows a very modest scatter, $< 15\%$, suggesting the enrichment process must be quite similar in all these massive systems. This is a

new finding and has significant implications on feedback processes. Together with results from thermodynamic properties presented in a previous X-COP paper, it affords a coherent picture where feedback effects do not vary significantly from one system to another. By combing ICM with stellar measurements we have found the amount of Fe diffused in the ICM to be about ten times higher than that locked in stars. Our estimates suggest, with some strenght, that the measured iron mass is well in excess of the predicted one. Although systematics errors, especially those associated to stellar masses, prevent us from making a defitive statement, a possible intriguing explanation of this discrepancy is that the ICM may be more compactly distributed than the stellar matter so that a fraction of the stars responsible of the enrichment of the ICM may lie beyond R_{500}.

The chemical evolution of galaxy clusters by measuring the iron mass in the ICM after dissecting the abundance profiles into different components using *Chandra* archival observations of 186 morphologically regular clusters in the redshift range of [0.04, 1.07] is investigated in Liu et al. (2020). We find that the iron plateau shows no evolution with redshift. On the other hand, we find a marginal ($< 2\sigma$ c.l.) decrease with redshift in the iron mass included in the iron peak rescaled by the gas mass. We also measure that the fraction of iron peak mass is typically a few percent of the total iron mass within R_{500}. Therefore, since the total iron mass budget is dominated by the plateau, we find consistently that the global gas mass-weighted iron abundance does not evolve significantly across our sample. Moreover, we confirm that past claims of evolution in the global iron abundance turn out to be due to the use of cluster samples with different selection methods combined with the use of emission-weighted, instead of gas mass-weighted, abundance values. Finally, while the intrinsic scatter in the iron plateau mass is consistent with zero, the iron peak mass exhibits a large scatter, in line with the fact that the peak is produced after the virialization of the halo and depends on the formation history of the hosting cool core and the strength of the associated feedback processes.
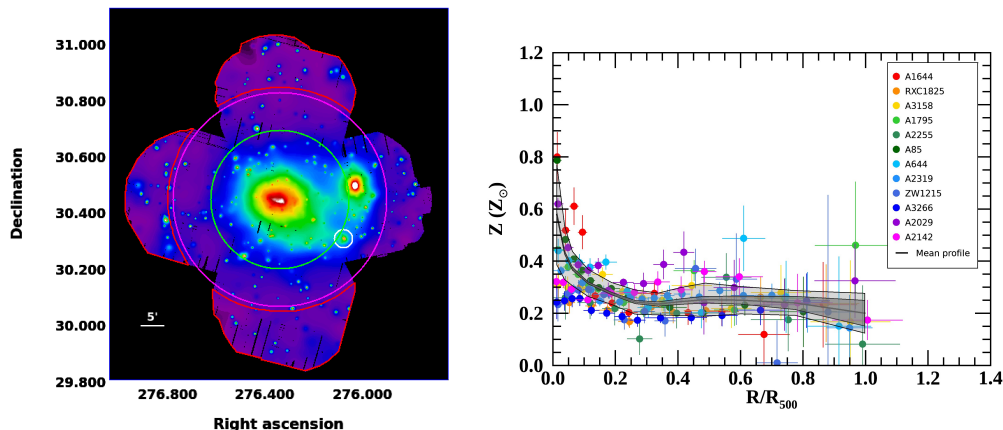
Fig. 3. (Left) *XMM-Newton* mosaic image of the Lyra cluster complex in units of counts/pixel in the 0.7-1.2 keV energy band. The cluster RXCJ1825 is in the center of the image with the green and magenta circles representing the location of its R_{500} and R_{200}, respectively. The cluster CIZAJ1824 is west of RXCJ1825, whereas the white circle is centered on the SG. Adapted from Clavico et al. (2019). (Right) Iron abundance profiles as a function of R/R_{500}. Abundance are measured solely through the Fe $K\alpha$ line. The dark and light shaded areas indicate respectively the statistical error and the total scatter. Adapted from Ghizzardi et al. (2021).

A central drop of ICM iron abundance has been observed in several cool-core clusters. It has been proposed that this abundance drop may be due, at least partially, to the depletion of Fe into dust grains in the central, high-density regions (e.g. Voit & Donahue , 2011). According to this scenario, noble gas elements such as Ar and Ne are not expected to be depleted into dust, and therefore should not show any drop, but follow the general increase of metal abundance toward the center. Liu et al. (2019) test this scenario by measuring with *Chandra* data the radial profiles of Ar and Ne in a sample of 12 groups and clusters where a central drop in Fe abundance has been detected. We recover the presence of the Fe drop in 10 out of 12 clusters at more than 2σ c.l., and 4 Ar drops with similar significance. This result is consistent with a scenario in which some fraction of Fe is depleted into dust grains in the inner regions, although the global central abundance drop is mostly due to mechanical processes, like the displacement of metal-rich ICM from the very center to larger radii by AGN-driven feedback.

On the role of AGN-driven feedback on different mass scales, Gaspari et al. (2019) carry out a comprehensive Bayesian correlation analysis between hot halos and direct masses of supermassive black holes (SMBHs), by retrieving the X-ray plasma properties (temperature, luminosity, density, pressure, and masses) over galactic to cluster scales for 85 diverse systems. We test the three major channels for SMBH growth: hot/Bondi-like models have inconsistent anticorrelation with X-ray halos and too low feeding; cosmological simulations find SMBH mergers as subdominant over most of cosmic time and too rare to induce a central-limit-theorem effect; the scalings are consistent with chaotic cold accretion, the rain of matter condensing out of the turbulent X-ray halos that sustains a long-term self-regulated feedback loop.

Sereno et al. (2018) reported the first detection of the correlated dark matter associated to a single cluster, PSZ2 G099.86+58.45 (see Fig. 4), obtained from the analysis of the environment bias in a sample of very massive clusters, selected through the SZ effect by the *Planck* mission. The system is extremely

rare in the current paradigm of structure formation. The gravitational lensing signal was traced up to 30 Mpc with high signal-to-noise ratio (~3.4). The measured shear is very large and points at environment matter density in notable excess of the cosmological mean.

The CLUMP-3D (CLUster Multi-Probes in Three Dimensions; Sereno et al. , 2017) project exploits rich data-sets to infer unbiased measurements of mass and concentration together with the intrinsic shape and the equilibrium status of galaxt clusters. The full three-dimensional Bayesian analysis combines strong (SL) and weak lensing (WL), X-ray surface brightness and temperature, and the SZ effect. In a nutshell, lensing constrains the 2D mass and concentration which are deprojected thanks to the shape and orientation information from X-ray and SZe. The ΛCDM model of structure formation makes strong predictions on the concentration and shape of dark matter (DM) halos, which are determined by mass accretion processes. In Sereno et al. (2018), we compare the predicted shapes with accurate and precise measurements from a a multi-probe 3D analysis of the X-ray regular Cluster Lensing and Supernova survey with Hubble (CLASH) clusters. The cluster shapes and concentrations are consistent with ΛCDM predictions. The CLASH clusters are randomly oriented, as expected given the sample selection criteria. Shapes agree with numerical results for DM-only halos, which hints at baryonic physics being less effective in making halos rounder. Sayers et al. (2021) report the non-thermal pressure fraction (P_{nt}/P_{tot}) obtained from a three-dimensional triaxial analysis of 16 galaxy clusters in the CLASH sample using gravitational lensing (GL) data primarily from Subaru and HST, X-ray spectroscopic imaging from *Chandra*, and SZ effect data from *Planck* and Bolocam. Our results span the approximate radial range $0.015 - 0.4R_{200m}$ (~ 35-1000 kpc; see Fig. 4). In the inner regions, the ensemble average P_{nt}/P_{tot} is consistent with zero with an upper limit of 9 per cent, indicating that heating from active galactic nuclei and other relevant processes do not produce significant deviations from the hydrostatic equilibrium between 0.015 and $0.1R_{200m}$. The ensemble average P_{nt}/P_{tot} increases outside of this radius to approximately 20 per cent at $0.4R_{200m}$, as expected from simulations, due to newly accreted material thermalizing via a series of shocks. Also in agreement with simulations, we find significant cluster-to-cluster variation in P_{nt}/P_{tot} and little difference in the ensemble average P_{nt}/P_{tot} based on dynamical state.

In Lovisari et al. (2020), we report the scaling relations derived by fitting the X-ray parameters determined from analyzing the *XMM-Newton* observations of 120 galaxy clusters in the *Planck* Early Sunyaev-Zel'dovich sample spanning the redshift range of $0.059 < z < 0.546$. We find that the slopes of all the investigated scaling relations significantly deviate from the self-similar predictions, if self-similar redshift evolution is assumed. When the redshift evolution is left free to vary, the derived slopes are more in agreement with the self-similar predictions. Relaxed clusters have on average about 30% higher X-ray luminosity than disturbed clusters at a given mass, a difference that, depending on the relative fraction of relaxed and disturbed clusters in the samples (e.g., SZ vs. X-ray selected), has a strong impact on the normalization obtained in different studies. For the first time, we find significant evolution ($> 3\sigma$) of the $M_{tot}-T$ relation, pointing to an increase of the kinetic-to-thermal energy ratio with redshift. This is consistent with a scenario in which higher-redshift clusters are on average more disturbed than their lower-redshift counterparts.

The same sample has been analyzed in Ettori et al. (2020b) to calibrate the predicted scaling laws between gas mass, temperature, luminosity, and total mass from their semi-analytic model based on a universal pressure profile in hydrostatic equilibrium within a cold dark matter halo with a defined relation between mass and concentration. This model allows also to quantify any deviation from the self-similar predictions in terms of temperature dependence of a few physical quantities such as the gas mass fraction, the relation between spectroscopic temperature and its global value, and, if present, the hydrostatic mass bias.

Sereno et al. have promoted the CoMaLit (COmparing MAsses in LITerature; Sereno
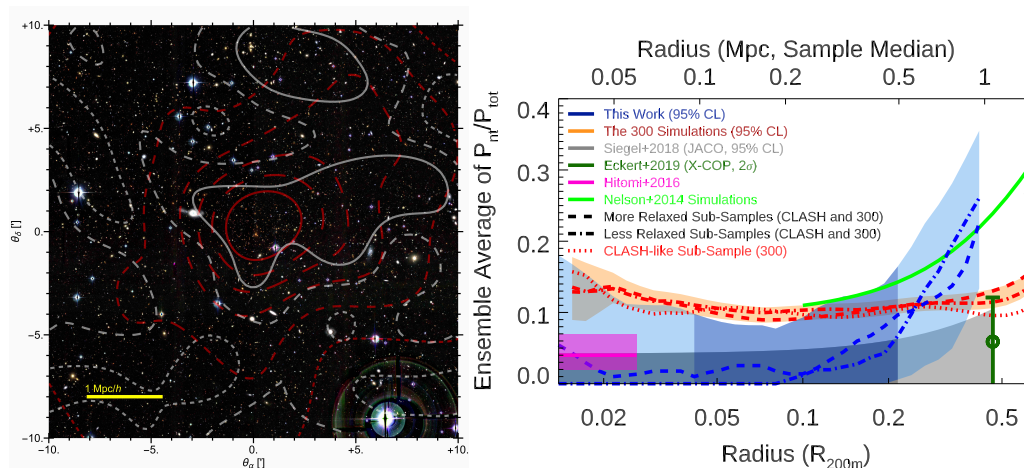
Fig. 4. (Left) Adapted from Sereno et al. (2018). Colour image of the region around PSZ2 G099.86+58.45. The contours show the mass distribution reconstructed from WL (white), and optical *i*-light of the galaxies with photometric redshift within ±0.06(1 + *z*) of the cluster redshift (red). The longer the dash, the higher the contour value. The map is centred on the Brightest Cluster Galaxy. North is up. (Right) Adapted from Sayers et al. (2021). Ensemble-average P_{nt}/P_{tot} from the analysis of 16 CLASH galaxy clusters. Lighter shading indicates regions where biases due to modeling systematics may exist. Dashed and dot-dashed lines indicate the most likely profiles for the more relaxed and less relaxed sub-samples of the CLASH galaxy clusters and the 300 simulations. The red dotted line shows the most likely profile from a CLASH-like selection of 20 objects from the 300 simulations.

& Ettori , 2015) series of papers, where we have applied Bayesian hierarchical procedures to studies of masses and scaling relations. The method can deal with heteroscedastic and possibly correlated measurement errors, intrinsic scatter, upper and lower limits, systematic errors, missing data, forecasting, time evolution, and selection effects. In the fifth paper of the series (Sereno & Ettori , 2017), we dealt with efficient mass forecasting. The method was extended to multi-dimensional analyses in Sereno et al. (2019). In CoMaLit-VI (Sereno et al. , 2020b), the intrinsic scatter of the mass proxy in stacked analyses of the weak lensing signal extracted from third data release of the Kilo-Degree Survey and associated to galaxy clusters detected with the AMICO (Adaptive Matched Identifier of Clustered Objects) algorithm.

On the scaling relations, we have played a relevant role in defining and assessing the physical properties of the galaxy groups and clusters selected in the *XXL* survey, that covers two areas of 25 deg² each with *XMM-Newton*

observations to a sensitivity of ∼ 5 × 10⁻¹⁵ erg s⁻¹ cm⁻² (for point sources). This project has produced about 15 refereed papers in the last 3 years on this topic. We mention here a few of those. In Adami et al. (2018), we present a catalog of 365 clusters, down to a flux of a few 10⁻¹⁵ erg s⁻¹ cm⁻² in the [0.5-2] keV band and in a 1' aperture. This release contains the complete subset of clusters for which the selection function is well determined plus all X-ray clusters which are, to date, spectroscopically confirmed. Sereno et al. (2020a) present the joint-analysis of multi-wavelength surveys - the *XXL* survey at *XMM-Newton* in the X-ray band, and the Hyper Suprime-Cam Subaru Strategic Program for optical weak lensing- to study an X-ray selected, complete sample of clusters and groups. The scalings of gas mass, temperature, and soft-band X-ray luminosity with the weak lensing mass show imprints of radiative cooling and active galactic nucleus feedback in group. Akino et al. (2021) combine HSC-SSP weak-lensing mass measurements, *XXL* X-ray gas mass measurements, and HSC and

SDSS multiband photometry to determine the baryon budget for a sample of 136 *XXL* galaxy groups and clusters spanning nearly two orders of magnitude in mass ($M_{500} \sim 10^{13} - 10^{15} M_{\odot}$) and the redshift range $0 < z < 1$. We carry out a Bayesian analysis of multivariate mass-scaling relations of gas mass, galaxy stellar mass, stellar mass of brightest cluster galaxies, and soft-band X-ray luminosity, by taking into account the intrinsic covariance between cluster properties, selection effect, weak-lensing mass calibration, and observational error covariance matrix. The mass-dependent slope of the gas mass–total mass relation is found to be steeper than the self-similar prediction of unity, whereas the slope of the stellar mass–total mass relation is shallower than unity. The baryon, gas mass, and stellar mass fractions as a function of M_{500} agree with the results from numerical simulations and previous observations. We successfully constrain the full intrinsic covariance of the baryonic contents, that do not show any redshift evolution.

3. The XMM Multi-Year Heritage Cluster Project: CHEX-MATE
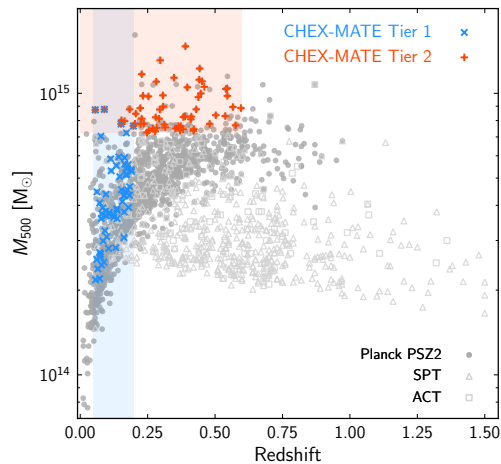
Fig. 5. Distribution in the $M_{500} - z$ plane of confirmed clusters from major SZE surveys, available at the time of proposal submission (October 2017). Adapted from CHEX-MATE collaboration (2021).

Building on the *Planck* All sky Sunyaev-Zel'dovich effect survey, we obtained in *XMM-Newton* AO17 3 Msec to follow-up 118 clusters, comprising an unbiased census of both the population of clusters at the most recent time ($z < 0.2$; Tier-1 in Fig. 5), and the most massive objects to have formed thus far in the history of the Universe (Tier-2). In particular, with this unique sample, our goals are to: (i) Assess the relative importance of gravitational and non-gravitational processes in shaping cluster properties. The densest core regions, where the interplay between cooling and central AGN feedback is strongest, provide key diagnostics on the impact of non-gravitational processes on the ICM. If cool cores are less prominent than previously thought from X-ray selected samples, we may have to fundamentally revise our vision of galaxy feedback at cluster scales. We will reassess the true distribution of cool core strength and its possible bimodality, and the amount of entropy excess (which records the non-gravitational energy input into the ICM) as a function of radius, mass, and, at the high mass end, redshift. We will definitively establish the relation between core properties and the bulk, including dynamical state (e.g. are cool cores essentially found in relaxed systems? To what extent are they destroyed by mergers?). We will establish the new, population-level, baseline to understand the interplay between gravitational heating, cooling and AGN feedback. The wide mass range of our sample is critical, the highest mass systems being dominated by gravitational heating and the lower mass systems being progressively more affected by non-gravitational input. The radial coverage, from the core to at least R_{500}, is equally important for sampling the relative impact of the different energetic processes. (ii) Probe the dynamical collapse of the gas on different scales A key issue is to what extent the gas is in equilibrium in the dark matter potential, as a function of mass and radius. This is linked to the presence of: turbulence in the ICM; non-thermal electrons (detectable in radio emission); shocks; bulk motion; and sub-clustering at all scales. XMM observations of our unbiased sample, covering a wide mass range including the most re-

cently formed "monsters", will provide key information. Objective morphological indicators (e.g centroid shifts, power ratios etc) will be provided by the X-ray imaging. An exciting new development is the use of surface brightness fluctuations to constrain the turbulence spectrum. Combining SZ and X-ray imagery will constrain gas clumpiness and the thermodynamical properties in the outskirts, as addressed in our X-COP project (Eckert et al. , 2019; Ghirardini et al. , 2019). We will correlate with radio surveys such as LOFAR, to link the dynamical indicators to the presence and extent of non-thermal energy contained in radio halos and relics. We will measure the probability density function of various key ICM parameters, their covariances, their dependence on mass, and study outliers in detail. The same measures will be extracted from numerical simulations to help to interpret the link between ICM covariances and outliers, the dynamical state and the feedback activity in clusters. These results will give completely new insights into the hierarchical formation process, and provide key information for our investigation of mass biases. (iii) Construct a consistent picture of cluster mass estimates. We will measure total mass profiles (out to at least R_{500}) for all objects using the hydrostatic equilibrium (HE) equation. The total HE mass will be compared to mass proxies such as Y_{SZ}, L_X or Y_X (the product of ICM mass and temperature). Most importantly, weak lensing data are already available for a significant fraction of the Heritage sample, especially at high mass.

At the momemt of writing (December 2021), few XMM observations are still missing, but we have already published a first paper on the goals and strategies of our project (CHEX-MATE collaboration , 2021). A website with updated information and some products delivered to the community from the CHEX-MATE collaboration is maintained at CHEX-MATE site. A first Media INAF press release has been published on May 2021.

References

Adami C. et al., 2018, A&A, 620, 5

Akino D. et al., 2021, PASJ in press

Baldi A.S. et al., 2019, A&A, 630, 121

Botteon A. et al., 2019, A&A, 630, 77

CHEX-MATE collaboration, 2021, A&A, 650, 104

Clavico S. et al., 2019, A&A, 632, 27

Cova F. et al., 2019, A&A, 628, 83

Eckert D. et al., 2017, Astron. Nachr., 338, 293

Eckert D. et al., 2019, A&A, 621, 40

Ettori S. et al., 2019, A&A, 621, 39

Ettori S. et al., 2020a, AN, 341, 210

Ettori S. et al., 2020b, A&A, 644, 111

Ettori S., Eckert D, 2022, A&AL, 657, L1

Gaspari M. et al., 2019, ApJ, 884, 169

Ghirardini V. et al., 2019, A&A, 621, 41

Ghizzardi S. et al., 2021, A&A, 646, 92

Girardi M. et al., 2020, A&A, 633, 108

Kozmanyan A. et al., 2019, A&A, 621, 34

Kravtsov A., Borgani S., 2012, ARAA, 50, 353

Liu A. et al., 2019, MNRAS, 485, 1651

Liu A. et al., 2020, A&A, 637, 58

Lovisari L. et al., 2020, ApJ, 892, 102

Sayers J. et al., 2021, MNRAS, 505, 4338

Sereno M., Ettori S., 2015, MNRAS, 450, 3633

Sereno M., Ettori S., 2017, MNRAS, 468, 3322

Sereno M. et al., 2017, MNRAS, 467, 3801

Sereno M. et al., 2018, ApJ, 860, L4

Sereno M. et al., 2018, Nature Astr., 2, 744

Sereno M. et al., 2019, A&A, 632, 54

Sereno M. et al., 2020a, MNRAS, 492, 4528

Sereno M. et al., 2020b, MNRAS, 497, 894

Sunyaev R. A., Zel'dovich Y. B. 1972, Comm. Astrophys. Space Phys., 4, 173

Voit G.M., 2005, RvMP, 77, 207

Voit G.M., Donahue M., 2011, ApJ, 738, L24